Supplemental Material (SM): Numerical study of the temperature-dependent magnetization and susceptibility of Tm^{3+} in $LiTmF_4$

Leila Mollabashi,[1] S. Jalali-Asadabadi,[1,*] Czesław Rudowicz,[2] Muhammed Acikgoz,[3] Zahra Ghasemi-Dorcheh,[1] Reyhaneh Ebrahimi-Jaberi,[1] Mahdi Jalali-Asadabadi,[1] Shahrbano Rahimi,[1] and Farhad Jalali-Asadabadi[1,4]

[1]*Department of Physics, Faculty of Physics, University of Isfahan (UI), Hezar Jerib Avenue, Isfahan 81746-73441, Iran*
[2]*Faculty of Chemistry, A. Mickiewicz University (AMU), 61-614 Poznań, Poland*
[3]*Department of Science, The State University of New York (SUNY) Maritime College, New York 10465, USA*
[4]*Physics Department, Faculty of Science, Razi University, Kermanshah, Iran*

This Supplemental Material (SM) accompanies the main paper titled "Temperature-dependent magnetization and susceptibility of Tm^{3+} in $LiTmF_4$: integrating DFT, crystal field, superposition model, and thermodynamic under an external magnetic field" and delves into the crystalline structure surrounding the Tm^{3+} ion in $LiTmF_4$. It presents data including positional parameters, bond lengths, and angular coordinates relevant to the ligands within the unit cell. Furthermore, this SM describes how non-interacting localized R^{3+} magnetic ions interact with an external magnetic field. It emphasizes the basic concepts of dipole interactions, Langevin and Brillouin functions, and sheds light on how these ions behave under different thermal and magnetic circumstances, highlighting the influence these factors have on the system's magnetization and susceptibility. The primary objective is to compare the results computed numerically for our interacting $LiTmF_4$ system in the presence of an external magnetic field discussed in the main paper with those derived analytically for a non-interacting model when exposed to an external magnetic field. We discuss the method used for investigating the non-interacting paramagnetic system, establishing it as an extreme reference point. We compare this with the results obtained for the interacting system, analyzed through the use of density functional theory (DFT) combined with crystal field theory (CFT), or DFT+CFT, complemented by statistical mechanics. At the extreme limit, the non-interacting system serves as a benchmark for validating our results, as we expect both the non-interacting and interacting systems to converge at this point. This comparison is crucial for checking the consistency and accuracy of our findings for the non-interacting system against the theoretical predictions for the interacting system. Consequently, this SM provides a thorough validation of the conclusions presented in the main paper. In the Van Vleck section, we further elucidate the nuances of Van Vleck paramagnetism, demonstrating its significance across various rare-earth ions and conditions. This section underscores the insights regarding the non-necessity of a zero ground state angular momentum for Van Vleck paramagnetism and its temperature-independent magnetic susceptibility inside crystalline environment, offering an understanding of the magnetic properties in complex systems.

SI. CRYSTAL STRUCTURE DATA USED FOR THE SPM/CFPs CALCULATIONS

In this section, we examine the $LiTmF_4$ crystal structure, as shown in Fig. S1. This figure divides into two parts: the basic unit cell of $LiTmF_4$ and the detailed area around the Tm^{3+} site, which can be seen from various directions due to different coordinate systems. The unit cell part of the image offers a glimpse into the complicated arrangement of atoms and the connections between them within the crystal. Understanding the shape of the unit cell, including the positions of atoms and the lengths of bonds between them, helps in figuring out how the crystal behaves overall. The Tm^{3+} site is a special spot in the structure where many important connections with nearby atoms happen. This site plays a role in determining the features of the $LiTmF_4$ material. The different orientations of the coordinate systems in the figure help us visualize these complex interactions more clearly and from various perspectives. These orientations provide a multi-faceted view, enabling a visualization of the interactions occurring at the microscopic level.

SII. SPM/CFPs CALCULATIONS

In this section, we concentrate on the calculations related to the superposition model (SPM) and crystal field parameters (CFPs), central to understanding the behavior of the Tm^{3+} ions in the $LiTmF_4$ crystal structure. In Table S1, we present details regarding the spatial relations between the central Tm atom and its adjacent fluoride (F) ligands, from F1 to F8, within the unit cell of the $LiTmF_4$ compound. Please note that all fluoride ions are equivalent, meaning they occupy symmetrical positions within the structure. The original Cartesian coordinates of these atoms are denoted as $(x/a, y/b, z/c)$, with reference to the respective lattice parameters where $a = b = 5.1450$ Å and $c = 10.6400$ Å. A significant portion of our analysis hinges upon the translation operation applied to the initial position of the Tm atom, which was previously positioned at $(0.50000, 0.25000, 0.37500)$. Through the application of a constant vector, we managed to reposition the Tm atom at the origin, leading to a change in the reference frame for the surrounding ligand atoms as well. The redefined coordinates, denoted as $(x'/a, y'/b, z'/c)$ in the table, serve to underscore the relative positions of the F ligands to the newly centered Tm atom. These relative coordinates are essential for our ensuing discussion on bond lengths and

* Corresponding author: sjalali@sci.ui.ac.ir

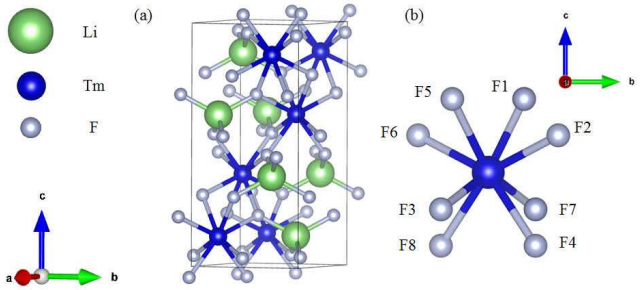

FIG. S1. The scheelite structure of the $LiTmF_4$ crystal. (a) Highlighted within the gray tetragonal crystal system is the conventional unit cell, illustrated alongside the respective coordinate axes. (b) This panel offers a closer look at the local structural arrangement at the Tm^{3+} site, where it is surrounded by 8 fluoride ligands, labeled F1 to F8, viewed from the 'a' direction. In this illustration, the green spheres represent Li ions, blue signifies Tm ions, and the gray ones denote F ions.

TABLE S1. The table depicts the relative positions of the Tm atom and its eight neighboring ligand atoms (F1 to F8) within the $LiTmF_4$ unit cell, denoted in Cartesian coordinates as $(x/a, y/b, z/c)$. The coordinate values are relative to the corresponding lattice parameters (a, b, c), where $a = b = 5.1450$ Å and $c = 10.6400$ Å. Additionally, a translation operation has been applied using a constant vector corresponding to the initial position of the Tm atom $(0.50000, 0.25000, 0.37500)$, repositioning the Tm atom to the origin. The positions post-translation are indicated as $(x'/a, y'/b, z'/c)$.

Bond	x/a	y/b	z/c	x'/a	y'/b	z'/c
Tm	0.50000	0.25000	0.37500	0.00000	0.00000	0.00000
F1	0.27685	0.41937	0.54122	-0.22315	0.16937	0.16622
F2	0.72315	0.58063	0.45878	0.33063	0.33063	0.08378
F3	0.83063	0.02685	0.29122	0.33063	-0.22315	-0.08378
F4	0.66937	0.47315	0.20878	0.16937	0.22315	-0.16622
F5	0.72315	0.08063	0.54122	0.22315	-0.16937	0.16622
F6	0.27685	-0.08063	0.45878	-0.22315	-0.33063	0.08378
F7	0.16937	0.47315	0.29122	-0.33063	0.22315	-0.08378
F8	0.33063	0.02685	0.20878	-0.16937	-0.22315	-0.16622

TABLE S2. Details of the bond lengths (R_i) in Å and spherical angles (θ_i and ϕ_i) in degrees between the central Tm atom and its surrounding 8 F ligands (F1 to F8), as utilized in Eq. 17 in the main paper. Refer to Fig. S1 for the visualization of the ML_n complex structure, where M represents the metal (Tm), L represents the ligand (F), and n indicates the number of ligands surrounding M (8). The R_i, θ_i, and ϕ_i in this table are found from the positions post-translation indicated as $(x'/a, y'/b, z'/c)$ in Table S1. All fluoride ions are equivalent.

Bond	R_i	θ_i	ϕ_i
(F1-Tm)	2.28156	39.1787	142.8016
(F2-Tm)	2.23752	66.5230	55.9837
(F3-Tm)	2.23752	113.4770	-34.0163
(F4-Tm)	2.28156	140.8213	52.8016
(F5-Tm)	2.28156	39.1787	-37.1984
(F6-Tm)	2.23752	66.5230	235.9837
(F7-Tm)	2.23752	113.4770	145.9837
(F8-Tm)	2.28156	140.8213	232.8016

TABLE S3. The crystal field parameters (CFPs), denoted as B_{kq}, computed utilizing the semiempirical superposition model (SPM) to align with the average CFPs presented in Table 1 of the main paper. The parameters were fitted based on the averaged data available in Table 1 of the main article.

Compound	B_{20}	B_{40}	B_{44}	B_{4-4}	B_{60}	B_{64}	B_{6-4}
$LiTmF_4$	373	-699	-619	555	39	-771	573
$LiYF_4$:Tm^{3+}	357	-630	-563	504	-47	920	-684

angles, as they present a clearer image of the spatial relationships and bonding configurations within the complex. As we can observe, the translated coordinates reveal a symmetrical distribution of ligands around the Tm atom, hinting at a probable geometrical structure which could be further analyzed for its properties and behavior. It is particularly interesting to note the symmetrical arrangement in the translated coordinates, indicating the ligands might be forming a highly ordered structure around the Tm atom.

The data showcased in Table S2 elucidates the bonding relationships between the central Tm atom and its adjacent 8 F ligands (F1 to F8), as encapsulated in the metal-ligand complex ML_n, visually represented in Fig. S1. Here, the Tm atom signifies the metal (M), and the F ligands embody the ligands (L) surrounding the metal, with 'n' denoting the count of these ligands, which is 8 in the present instance. A deeper inspection of the bond lengths (R_i) in Å, and the spherical angles (θ_i and ϕ_i) in degrees present a perspective on the geometrical nuances of the complex. The bond lengths are consistent, showing two distinct groups; the (F2-Tm), (F3-Tm), (F6-Tm), and (F7-Tm) bonds have a length of 2.23752 Å while the (F1-Tm), (F4-Tm), (F5-Tm), and (F8-Tm) bonds are slightly longer, measured at 2.28156 Å. When it comes to spherical angles, we notice significant variations which point towards a complex, possibly non-symmetrical, geometric structure. The θ_i values range from 39.1787° to 140.8213°, and ϕ_i values are spread across a wide range, indicating a rich three-dimensional geometric structure. These bonding parameters play an indispensable role in Equation 17, outlined in the main paper, where they are derived from the transformed coordinates $(x'/a, y'/b, z'/c)$, detailed in Table S1. To understand the intricate details of these relations and the potential implications it has on the crystal structure surrounding the Tm^{3+} ion, a thorough analysis of the positional parameters detailed in Table S1 is warranted. This will provide a more holistic view of the interactions and the spatial arrangement within the metal-ligand complex.

Following the structural analysis, we present the results of our SPM/CFPs calculations. The parameters $\bar{A}_2(R_0)$, $\bar{A}_4(R_0)$, and $\bar{A}_6(R_0)$, alongside the values of t_2, t_4, and t_6 have been calculated to be in alignment with general trends observed in the literature, showcasing the validity of our model. These trends are clearly represented as $\bar{A}_2(R_0) > \bar{A}_4(R_0) > \bar{A}_6(R_0)$ and $t_2 < t_4 < t_6$. The reference distance adopted in our calculations is $\mathbf{R}_0 = \mathbf{R}_{avg} = 2.2595$ Å.

We have successfully derived all 7 CFPs for the S4 (Tetrag-

onal II) local site symmetry found at Tm^{3+} centers, the details of which are documented in Table S3. Notably, the parameters $B20$, B_{40}, and B_{60} align well with the average values tabulated in Table I of the main paper. This third table illustrates the calculated CFPs (B_{kq}) based on the SPM, showing a match satisfactorily with the average CFPs found in Table I.

Furthermore, we believe that these derived SPM model parameters are not confined to the study of $LiTmF_4$ crystal but can be applied to similar systems encompassing F-ligands complexes, thus widening the scope and applicability of our findings.

SIII. NON-INTERACTING ENSEMBLE OF LOCALIZED R^{3+} MAGNETIC IONS IN MAGNETIC FIELD

Simulating paramagnetism can introduce challenges due to the inherent difficulties in presenting noncollinear magnetism accurately using the standard collinear methods available in the density functional theory (DFT) based codes such as WIEN2k code [1]. These complexities necessitate the use of more advanced and time-consuming techniques such as the noncollinear magnetism version of the WIEN2k code, embodied into the WIENncm code [2], or the application of DFT augmented with dynamic mean-field theory (DFT+DMFT), a feature implemented in the embedded DMFT (eDMFT) code [3]. However, as observed in our recent work [4], these techniques come with a high computational cost. To this end, we utilize the DFT plus crystal field theory (CFT), DFT+CFT, method paired with statistical mechanics to investigate the properties of this insulating Van Vleck paramagnetic compound.

In this section, we focus on analyzing an ensemble of non-interacting localized R^{3+} magnetic ions under the influence of an external magnetic field, adopting a statistical mechanics approach within a canonical ensemble framework. This non-interacting system serves as a theoretical benchmark, representing an extreme limit scenario for our $LiTmF_4$ system under study, as elaborated in the main paper. It is noteworthy that our main paper explores the paramagnetic $LiTmF_4$ system in a similar manner to this non-interacting system, applying statistical methods to investigate the paramagnetic phase of the system. A key distinction between the two studies resides in the method employed to evaluate the energies involved. For the non-interacting system, we are able to derive energies analytically due to its straightforward nature, an approach not feasible with the interacting system. In contrast, the interacting system demands the utilization of the DFT+CFT approach to derive energies, forming the basis for constructing the canonical partition function, a crucial step in computing the magnetic moment. In fact, this section aims to elucidate how the statistical mechanics method applied to non-interacting paramagnetic systems can be extended to analyze interacting systems. Additionally, it intends to establish the findings of the interacting system as an extreme reference point for comparison with the results garnered through the DFT+CFT+"Statistical Mechanics" approach for the interacting system, see Figs. 2 and 3 of the main paper.

We consider a system of non-interacting N localized magnetic dipoles $\boldsymbol{m}$ in an external magnetic field B. On the other words we only pay attention into the interaction between dipoles and external magnetic field. The energy of dipoles is [5]:

$$\varepsilon = -\sum_i^N \varepsilon_i = -\sum_i^N \boldsymbol{m}.\boldsymbol{B} = -\boldsymbol{m}B\sum_i^N \cos\theta_i, \tag{S1}$$

where θ_i is the angle between magnetic dipole and external magnetic field. The partition function is

$$Q_N = Q_1^N, \tag{S2}$$

where

$$Q_1 = \sum_\theta \exp(\beta \boldsymbol{m}B\cos\theta), \tag{S3}$$

where β is $1/k_BT$ and k_B is the Boltzmann constant. In the classical point of view

$$\begin{aligned} Q_1 &= \int_{\theta_0=0}^{2\pi}\int_{\varphi_0=0}^{\pi} \exp(\beta\boldsymbol{m}B\cos\theta)\sin\theta d\theta d\varphi \\ &= 4\pi\frac{\sinh(\beta\boldsymbol{m}B)}{\beta\boldsymbol{m}B}, \end{aligned} \tag{S4}$$

The mean magnetic moment of the system is

$$\begin{aligned} M_z &= \frac{N}{\beta}\frac{\partial}{\partial B}\ln Q_1(\beta) \\ &= N\boldsymbol{m}L(\beta\boldsymbol{m}B), \end{aligned} \tag{S5}$$

weher $L(x)$ is Langevin function and x is $\beta\boldsymbol{m}B$.

$$L(x) = \coth(x) - \frac{1}{x}. \tag{S6}$$

For $x \gg 1$, the L(x) approaches to unity, and for $x \ll 1$, the $L(x)$ $x/3 - x^3/45$. The latter $L(x)$ gives the susceptibility in the lowest approximation $\chi = C/T$ where C is curie constant.

For free atoms or ions, the Zeeman Hamiltonian is

$$\hat{H}_Z = \mu_B g\boldsymbol{B}.\boldsymbol{J}, \tag{S7}$$

where $\boldsymbol{J}$ is the total angular momentum number and g is the Landé's g-factor [6] which can be written as:

$$g = \frac{J(J+1)(g_L+g_S) + \{L(L+1) - S(S+1)\}(g_L - g_S)}{2J(J+1)}, \tag{S8}$$

If $g_L = 1$ and $g_S = 2$, then it can be simplified as:

$$g = \frac{3}{2} + \frac{S(S+1) - L(L+1)}{2J(J+1)}, \tag{S9}$$

where S, L, and J are the spin, orbital and quantum numbers, respectively. The Landé factor reduces to 2 (1), if the net angular momentum of the rare earth ion is due solely to electron spins (orbitals); *viz.* $g\,(S, L=0, J) = \frac{3}{2} + \frac{S(S+1)-0}{2S(S+1)} = \frac{3}{2} + \frac{1}{2} = \frac{4}{2} = 2$ ($g\,(S=0, L, J) = \frac{3}{2} + \frac{0-L(L+1)}{2L(L+1)} = \frac{3}{2} - \frac{1}{2} = \frac{2}{2} = 1$).

There are the following relations between $g\,(S,L,J)$, **S**, **L**, and **J** = **L** + **S**:

$$\begin{aligned} \boldsymbol{L} &= \big(2 - g\,(S,L,J)\big)\,\boldsymbol{J}, \\ \boldsymbol{S} &= \big(g\,(S,L,J) - 1\big)\,\boldsymbol{J}, \\ \boldsymbol{L} + 2\boldsymbol{S} &= g\,(S,L,J)\;\;\boldsymbol{J}. \end{aligned} \tag{S10}$$

It is worth to highlight that the g-factor in atoms, as defined and used in this SM document, and the g-tensor in the context of crystal fields in solids, as defined in Sec. II A and calculated and discussed in Sec. IV D of the main text, refer to related but distinct concepts, primarily differing in their application and complexity due to the environment surrounding the atoms or ions.

The g-factor in atoms is a dimensionless quantity that characterizes the magnetic moment and angular momentum of an atom or a free particle. It is typically used in the context of free atoms or particles where the electronic environment is relatively simple and spherically symmetric. The g-factor is often associated with the Zeeman effect, where it describes how atomic energy levels split under an applied magnetic field. it is a scalar quantity, meaning it has magnitude but no direction, and is usually denoted simply as g.

The g-tensor in solid-state physics, particularly in the context of crystal fields, refers to a tensorial generalization of the atomic g-factor. In crystals, the electronic environment of atoms or ions can be anisotropic due to the crystal field (the effect of the electric fields of surrounding ions). This anisotropy leads to the g-factor becoming a tensor (the g-tensor), meaning it varies depending on the direction in the crystal lattice. The g-tensor is a 3×3 matrix that reflects the anisotropic nature of the magnetic interactions in the solid. It is essential for describing phenomena like electron paramagnetic resonance (EPR) or magnetic resonance imaging (MRI) in solid materials. The components of the g-tensor give information about how the magnetic properties, like the magnetic moment and Zeeman splitting, vary with the direction of the applied magnetic field in the crystal lattice.

In summary, while the atomic g-factor is a simpler, scalar quantity used for free atoms or particles, the g-tensor in crystal fields is a more complex, matrix-based representation that accounts for the directional dependence of magnetic properties in the anisotropic environment of a solid-state crystal.

The relation between magnetic dipole moment $\boldsymbol{m}$ and its angular momentum $\boldsymbol{J}$ for free atom or ion is:

$$\boldsymbol{m} = \left(g\frac{e}{2\mathfrak{m}_e c}\right)\boldsymbol{J}, \tag{S11}$$

where $\mathfrak{m}_e$ is the mass of electron, c is the light velocity. By considering the z axes in the direction of magnetic field the component of magnetic moment in the direction of the magnetic field will be:

$$m_z = g\mu_B m_J, \tag{S12}$$

where m_J is the magnetic quantum number. The energy of the dipole in the magnetic field **B** is:

$$\varepsilon = -\boldsymbol{m}.\boldsymbol{B}. \tag{S13}$$

From the following single-dipole partition function:

$$Q = \sum_{m_J=-J}^{J} \exp(\beta g \mu_B B m_J), \tag{S14}$$

the z component of magnetic moment M_z can be obtained as:

$$M_z = \frac{N}{\beta}\frac{\partial}{\partial B}\ln Q. \tag{S15}$$

Thus, the z component of the magnetic moment of a single dipole is:

$$M_z = g\mu_B J B_J(x), \tag{S16}$$

where $B_J(x)$ is the Brillouin function [5]

$$B_J(x) = \left(1 + \tfrac{1}{2J}\right)\coth\left[\left(1 + \tfrac{1}{2J}\right)x\right] - \tfrac{1}{2J}\coth\left[\tfrac{1}{2J}x\right], \tag{S17}$$

where $x = \beta g \mu_B J B$. The Brillouin function, which is parametrically dependent on J, can be represented across a range of J values, demonstrating specific asymptotic behaviors. Notably, in the limit as J approaches infinity, the Brillouin function converges to the classical Langevin function, denoted as $\mathrm{B}_\infty(x) = L(x)$, as expressed in Eq. (S6). Conversely, for $J = \frac{1}{2}$, it simplifies to the hyperbolic tangent function, expressed as $\mathrm{B}_{1/2}(x) = \tanh(x)$, illustrating the function's versatility in modeling magnetic response.

In strong field and low temperature $B_J(x) \simeq 1$. If $g\mu_B JB$ is small compared to the $k_B T$ at high temperatures and/or weak fields, the magnetic susceptibility is constant and given by Curie's law:

$$\chi_B = \frac{M}{B} = \frac{g^2\mu_B^2 J(J+1)}{3k_B T}\frac{N}{V} \equiv \frac{C}{T}. \tag{S18}$$

The temperature dependence of magnetic moment and susceptibility for Tm^{3+} ion in $LiTmF_4$ is discussed in subsection E of the main paper. Specifically, in Figs. 2 and 3, we show the changes in magnetization and magnetic susceptibility with respect to temperature variations, under the influence of a 0.1 T external magnetic field, utilizing our DFT+CFT/SPM method. Moreover, In Figs. 2 and 3 of the main paper, we analyze the changes in magnetization and magnetic susceptibility as functions of temperature. These analyses are based on two separate approaches: one involves a non-interacting ensemble of localized R^{3+} magnetic ions influenced by a magnetic field, and the other is based on a Hamiltonian that describes the behavior of magnetic ions within the crystal structure subjected to an external magnetic field. Furthermore, we compared the magnetic susceptibility behaviors of both models with experimental data, as shown in Figs. 2 and 3 of the main paper, and discussed in subsection D. At high temperatures, both models approach well to the experimental data, however, at lower temperatures, the interacting model yields more accurate results.

SIV. VAN VLECK PARAMAGNETISM

In this section, we aim to discuss that Van Vleck paramagnetism can occur even if the total angular momentum J is nonzero, and it can depend on temperature within a crystalline environment at high temperatures.

According to Eq. (2.47) of Ref. [7], when J is zero in the ground state, the system exhibits no paramagnetic effect, indicating that applying a magnetic field does not alter the ground state energy, hence no paramagnetic susceptibility. This statement holds true within the realm of first-order perturbation theory. However, second-order perturbation theory suggests a modification in the ground state energy E_0, due to the inclusion of excited states. This alteration for an ion with $J = 0$ is captured by Eq. (2.48) in Ref. [7], which considers both diamagnetic contributions and the interaction with excited states. The formula for magnetic susceptibility is expressed in Eq. (2.49) of Ref. [7] as:

$$\chi = \frac{N}{V}\left(2\mu_{\mathrm{B}}^2 \sum_n \frac{\left|\left\langle 0\left|\left(L_z + gS_z\right)\right|n\right\rangle\right|^2}{E_n - E_0} - \frac{e^2\mu_0}{6m_{\mathrm{e}}}\sum_{i=1}^{Z}\left\langle r_i^2\right\rangle\right), \tag{S19}$$

where the first term relates to Van Vleck paramagnetism and the second to conventional diamagnetic susceptibility, both described as small and temperature-independent, aligning with the discussions in Eq. 2.15 of Ref. [7].

In discussing the nuances of Van Vleck paramagnetism, two critical insights emerge. Firstly, the zero ground state angular momentum ($J = 0$) is not a prerequisite for Van Vleck paramagnetism. This distinction is supported by experimental and empirical observations, highlighting the depth and versatility of paramagnetic behaviors. The Van Vleck effect is crucial for understanding the magnetic properties of rare-earth ions, particularly in cases like Eu^{3+}, which exhibits a nonmagnetic ground state with $J = 0$ and an excited state with $J = 1$ at 330 K, contributing to paramagnetic susceptibility as shown in Table 4.5 of Ref. [8]. However, this effect is not limited to Eu^{3+}; it is also significant for other rare-earth ions. For example, Sm^{3+}, with a $J = 5$ ground state, has a closely lying excited state with $J = 7/2$ at 1225 K. Furthermore, the Van Vleck effect has been experimentally observed for Tm^{3+} ion with $J = 6$ in $LiTmF_4$ at low temperatures and high magnetic fields, as reported by Abubakirov *et al.* [9], highlighting its relevance across a variety of compounds and conditions. Therefore, the significance of taking into account the excited J-multiplets for the Tm^{3+} ion within the studied compound is crucial by the Van Vleck paramagnetism observed. Secondly, this paramagnetism exhibits temperature-independent magnetic susceptibility at low temperatures and in dilute systems, a hallmark of quantum mechanical effects. Conversely, at elevated temperatures or within a crystalline field, susceptibility may become temperature-dependent, underscoring the complex interplay between thermal energy and electronic states. Abubakirov *et al.* [9] experimentally and empirically studied temperature dependencies of magnetization in $LiTmF_4$ in two key orientations: within the (001) plane at angles corresponding to maximum and minimum susceptibility, $\phi = \phi_{\max}$ and $\phi_{\min}$, and along the [001] axis. Consistent with theoretical predictions for dilute crystals, the magnetization remained constant below 8 K, underscoring the characteristic temperature independence of Van Vleck paramagnets. Notably, along the [001] axis, magnetization exhibited a nonmonotonic temperature relationship, a common trait among Van Vleck paramagnets in orientations of minimal susceptibility. This behavior is attributed to the larger magnetic moments of magnetic ions in excited crystal field (CF) states. The observed temperature independence below 8 K also indicates a minimal presence of impurities, which would otherwise introduce conventional paramagnetism. The referenced studies on Tm^{3+} ions in $LiTmF_4$ [9], YVO_4 [10], and $LiYF_4$ [11] lattices provide a theoretical and experimental basis for understanding the temperature-independent magnetization below 8 K and nonmonotonic temperature dependence observed in $LiTmF_4$. These behaviors are characteristic of Van Vleck paramagnets, explained by the larger magnetic moments of Tm^{3+} ions in excited crystal field states. The connection highlights the crucial role of crystal field parameters in determining the magnetic and thermal properties of such materials, emphasizing the purity of the samples and the minimal influence of conventional paramagnetism.

In summary, Van Vleck paramagnetism is not limited to $J = 0$. The characteristic temperature independence of Van Vleck paramagnetism can occur in dilute gases at low temperatures, while it may exhibit temperature dependence within crystalline environments at higher temperatures.

LIST OF ABBREVIATIONS

Abbreviation	**Definition**
DFT	Density Functional Theory
CF	Crystal Field
CFT	Crystal Field Theory
CFPs	Crystal Field Parameters
DMFT	Dynamical Mean Field Theory
eDMFT	embedded Dynamical Mean Field Theory
DFT+DMFT	Density Functional Theory + Dynamical Mean Field Theory
SPM	Superposition Model
CQs	Conserved Quantities
SM	Supplemental Material (SM)
MCFT	Multiple Correlated Fitting Technique
FP-APW	Full-Potential Augmented Plane Waves
Exp.	Experimental
Emp.	Empirical
Δ	Hybridization Parameter
T	Tesla
Vv	Van Vleck
Reg.	Regression
Zeem.	Zeeman
DFT+CFT+Δ+Zeem.+Reg.	Density Functional Theory + Crystal Field Theory + Hybridization Parameter + Zeeman Effects + Regression

SPM+CFT+Δ+Zeem.+Reg.	Superposition Model + Crystal Field Theory + Hybridization Parameter + Zeeman Effects + Regression

[1] P. Blaha, K. Schwarz, G. K. H. Madsen, D. Kvasnicka, J. Luitz, R. Laskowski, F. Tran, and L. D. Marks, Wien2k, WIEN2k, An Augmented Plane Wave + Local Orbitals Program for Calculating Crystal Properties, Karlheinz Schwarz, Technische Universität Wien, Vienna, Austria, ISBN 3-9501031-1-2 (2021).

[2] R. Laskowski, G. K. H. Madsen, P. Blaha, and K. Schwarz, Magnetic structure and electric-field gradients of uranium dioxide: An ab initio study, Phys. Rev. B **69**, 140408(R) (2004).

[3] K. Haule, Exact double counting in combining the dynamical mean field theory and the density functional theory, Phys. Rev. Lett. **115**, 196403 (2015).

[4] M. Yazdani-Kachoei, S. Rahimi, R. Ebrahimi-Jaberi, J. Nematollahi, and S. Jalali-Asadabadi, Thermoelectric properties plus phonon and de haas–van alphen frequencies, Scientific Reports **12** (2022).

[5] R. Pathria, *Statistical Mechanics* (Elsevier Science, 2016).

[6] A. Abragam and B. Bleaney, *Electron Paramagnetic Resonance of Transition Ions*, International series of monographs on physics (Clarendon Press, 1970).

[7] S. Blundell, *Magnetism in Condensed Matter*, Oxford Master Series in Condensed Matter Physics (Oxford University Press Inc., New York, 2001).

[8] J. Coey, *Magnetism and Magnetic Materials*, Magnetism and Magnetic Materials (Cambridge University Press, 2010).

[9] D. I. Abubakirov, K. Matsumoto, H. Suzuki, and M. S. Tagirov, Anisotropic magnetization of the van vleck paramagnet $LiTmF_4$ at low temperatures and high magnetic fields, Journal of Physics: Condensed Matter **20**, 395223 (2008).

[10] V. Kumar, Vishwamittar, and K. Chandra, On the behaviour of the Tm^{3+}ion in YVO_4 $LiYF_4$, Journal of Physics C: Solid State Physics **10**, 267 (1977).

[11] C. Xueyuan and L. Zundu, Crystal-field analysis of the spectroscopic characteristics and magnetic properties of in crystal, Journal of Physics: Condensed Matter **9**, 4197 (1997).